

Long Term Motion Prediction Using Keyposes

Sena Kiciroglu¹ Wei Wang^{1,2} Mathieu Salzmann^{1,3} Pascal Fua¹

¹ CVLab, EPFL, Switzerland

² University of Trento, Italy

³ ClearSpace, Switzerland

Abstract

Long term human motion prediction is essential in safety-critical applications such as human-robot interaction and autonomous driving. In this paper we show that to achieve long term forecasting, predicting human pose at every time instant is unnecessary. Instead, it is more effective to predict a few keyposes and approximate intermediate ones by linearly interpolating the keyposes.

We will demonstrate that our approach enables us to predict realistic motions for up to 5 seconds in the future, which is far larger than the typical 1 second encountered in the literature. Furthermore, because we model future keyposes probabilistically, we can generate multiple plausible future motions by sampling at inference time. Over this extended time period, our predictions are more realistic, more diverse and better preserve the motion dynamics than those state-of-the-art methods yield.

1. Introduction

Human motion prediction is a key component of many vision-based applications, such as automated driving [11, 16, 34], surveillance [19, 30], accident prevention [37], and human-robot interaction [7, 14]. Its goal is to forecast the future 3D articulated motion of a person given their previous 3D poses. Most approaches formulate this task as one of regressing a person’s pose in every future frame of a sequence given the current ones. Recurrent neural networks [13, 28] and graph convolutional networks [21, 26, 27] have proven effective for this, at least for short-term predictions typically up to one second in the future. However, beyond one second the predictions degrade quickly and very little work has aimed to address this shortcoming.

This paper focuses on longer-term predictions. Our key insight is that predicting the pose in *every* future frame is unnecessary because, given two poses separated by a short time interval, one can easily guess the intermediate ones using simple linear interpolation. It is enough to predict a sequence of keyposes from which all others can be recovered by interpolation. Therefore instead of considering the

motion as a sequence of consecutive poses, we downsample it to a special set of “keyposes” from which all other poses can be linearly interpolated up to a fixed precision. We then utilize these keyposes for long-term motion prediction.

While all keyposes are unique, some of them tend to be similar to each other, which allows us to cluster them. Predicting future motions can then be reformulated as jointly classifying the cluster label of future keyposes and transition time between them. To this end, we design an RNN-based motion prediction network that takes earlier keyposes as input and yields a probability distribution over the clusters for each future keypose along with transition times. As a result, we can not only predict the most likely future motion by maximizing cluster probabilities but also generate multiple potential sequences by sampling these probability distributions. This is useful because people are not entirely predictable even when one knows what they have already done, as in the case of a pedestrian standing on the curb who may, or may not, cross the street.

In summary, our contributions are threefold:

- We introduce a keypose extraction algorithm to represent human motion in a compact way.
- We formulate motion prediction as a classification problem and design a framework to predict keypose label and durations.
- We demonstrate that our approach enables us to predict multiple realistic motions for up to 5 seconds in the future, which is far larger than the typical 1 second encountered in the literature. The motions we generate preserve the dynamic nature of the observations, whereas the methods designed for shorter timespans tend to degenerate towards static poses.

2. Related Work

The complexity of human motion makes deep learning an ideal framework for tackling the task of motion prediction. In this section, we first review the two main classes of deep models that have been used in the field and then discuss approaches that depart from these main trends. Finally, we discuss the use of keyposes for different tasks.

2.1. Human Motion Prediction using RNNs

Recurrent neural networks (RNN) are widely used architectures for modeling time-series data, for instance for natural-language processing [41] and music generation [35, 36]. Since the work of Fragkiadaki *et al.* [12], these architectures have become highly popular for human motion forecasting. In this context, the S-RNN of Jain *et al.* [18] transforms spatio-temporal graphs to a feedforward mixture of RNNs; the Dropout Autoencoder LSTM (DAE-LSTM) of Ghosh *et al.* [13] synthesizes long-term realistic looking motion sequences; the recent Generative Adversarial Imitation Learning (GAIL) of Wang *et al.* [39] was employed to train an RNN-based policy generator and critic networks. HP-GAN [3] uses an RNN-based GAN architecture to generate diverse future motions of 30 frames.

Despite their success, using RNNs for long-term motion prediction suffers from drawbacks. As pointed out by Martinez *et al.* [28] they tend to produce discontinuities at the transition between observed poses and predicted ones and often yield predictions that converge to the mean pose of the ground-truth data in the long term. In [28], this was circumvented by adding a residual connection so that the network only needs to predict the residual motion. Here, we also develop an RNN-based architecture. However, because we treat keypose prediction as a classification task, our approach will not suffer from the accumulated error that such models tend to generate when employed for regression.

2.2. Human Motion Prediction using GCNs

Mao *et al.* [27] proposed to overcome the weaknesses of RNNs by encoding motion in discrete cosine transform (DCT) space, to model temporal dependencies, and learning the relationships between the different joints via a GCN. Lebailly *et al.* [21] build on top of this work by combining a GCN architecture with a temporal inception layer. The temporal inception layer serves to process the input at different subsequence lengths, so as to exploit both short-term and long-term information. Alternatively, “History Repeats Itself” [26] combines the GCN architecture with an attention module aiming to learn the repetitive motion patterns. These methods constitute the state of the art for long-term prediction. Nevertheless, they were only showcased for forecasting up to 1 second in the future. As will be shown by our experiments, for longer timespans, they tend to degenerate to static predictions.

2.3. Other Human Motion Prediction Approaches

Several other architectures have been proposed for human motion prediction. For example, Bütepage *et al.* [6] employ several fully-connected encoder-decoder models to encode different properties of the data. One of the models is a time-scale convolutional encoder, with different filter sizes. In [7], a conditional variational autoencoder (CVAE)

is used to probabilistically model, predict and generate future motions. This probabilistic approach is extended in [8] to incorporate hierarchical action labels. Aliakbarian *et al.* [2] also perform motion generation and prediction by encoding their inputs using a CVAE. They are able to generate diverse motions by randomly sampling and perturbing the conditioning variables. Similarly, Yuan *et al.* [40] also use a CVAE based approach to generate multiple futures. Li *et al.* [22] use a convolutional neural network for motion prediction, producing separate short-term and long-term embeddings. In [1, 10], interactions between humans and objects in the scene are learned for context-aware motion prediction, which is beyond our scope. As a different task, several works generate realistic motions by conditioning on the action label, rather than the past motion [15, 32]. In any event, all the above-mentioned methods aim to regress the future poses at every time instant. Here, we will show that this is unnecessary, and that truly long-term prediction can be achieved more accurately by focusing the prediction on the essential poses, or keyposes, in a sequence.

2.4. Keyposes Applied to Other Tasks

Keyposes have been used for different tasks, such as action recognition. For example, in [25], 2D keyposes are used for single view action recognition. In [24], Adaboost is used to select keyposes that are discriminative for each action. In [5], linear latent low dimensional features extracted from sequences for action recognition and action prediction. Meanwhile [20] focus on generating realistic transitions between nodes on a motion graph, which resembles our notion of keyposes, to synthesize short animated sequences. However, none of these works predict future keyposes given past ones. To the best of our knowledge, our approach is first to use keyposes for long-term motion prediction.

3. Methodology

Classically, the task of motion prediction is defined as producing the sequence of 3D poses from $t = 1$ to $t = N$, denoted as $\mathbf{P}_{1:N}$, given the sequence of poses from $t = -M$ to $t = 0$, denoted as $\mathbf{P}_{-M:0}$. Each pose value \mathbf{P}_t is of dimension $3 \times J$, where J is the total number of joints. Therefore, pose-to-pose prediction can be written as

$$\mathbf{P}_{1:N} = F(\mathbf{P}_{-M:0}),$$

where F is the prediction function.

Our approach departs from this classical formalism by predicting keyposes from keyposes. A keypose \mathbf{K}_i is defined as a triplet containing a keypose value, label and duration, denoted as (\mathbf{V}_i, l_i, d_i) , where $i \in [1, I]$, and I is the total number of keyposes in a sequence. Each keypose value \mathbf{V}_i is of dimension $3 \times J$. Let us assume for now that we have extracted keypose values for the training data, and

that we have clustered these keypose values into C clusters. We will discuss in Section 3.1 our approach to doing so. Then, the keypose label $l_i \in [1, C]$ indicates which cluster the keypose falls into. Finally, the duration d_i is the number of transition frames from \mathbf{K}_{i-1} to \mathbf{K}_i .

Therefore, our keypose-to-keypose framework takes as input a motion $\mathbf{P}_{-M:0}$ defined by its keyposes $\mathbf{K}_{-I_1:0}$, where I_1 is the number of keyposes in the past sequence. We then aim to predict $\mathbf{K}_{1:I_2}$, where I_2 is the number of keyposes in the future sequence. We write this as

$$\mathbf{K}_{1:I_2} = G(\mathbf{K}_{-I_1:0}),$$

where G is the keypose-to-keypose prediction function.

In practice, we do not predict the keypose values $\mathbf{V}_{1:I_2}$, but only the labels $l_{1:I_2}$. To then obtain the d_{i+1} poses between keyposes \mathbf{K}_i and \mathbf{K}_{i+1} , we perform linear interpolation between the keypose cluster centers \mathbf{C}_{l_i} and $\mathbf{C}_{l_{i+1}}$. This yields

$$\mathbf{P}_{\Delta t+t} = \mathbf{C}_{l_i} + \Delta t \frac{\mathbf{C}_{l_{i+1}} - \mathbf{C}_{l_i}}{d_{i+1}},$$

where t is the time index of keypose \mathbf{K}_i in the sequence.

Note that we use a 3D joint position representation of human motion. This representation has been gaining popularity over Euler angles, due to the latter suffering from ambiguities. Specifically, two different sets of angles can represent the same pose. Consequently, the interpolation between poses represented by angles becomes ambiguous as well. Recent approaches have tried to solve this by changing the encoding to quaternions [31], but many works nonetheless report results using the 3D joint position representation [21, 26, 27].

3.1. Keyposes

Given a sequence of poses \mathbf{P}_t , $t \in [1, T]$ where T is the length of the sequence, we seek to retrieve the keyposes \mathbf{K}_i , $i \in [1, I]$. We employ an optimization based strategy to determine the poses which minimizes the L2 error between the original sequence \mathbf{P} and the sequence reconstructed by linear interpolation.

Our method is as follows:

- We set \mathbf{P}_1 and \mathbf{P}_T to be keyposes.
- We recursively subdivide the time window spanned by \mathbf{P} , where each split selects the pose \mathbf{P}_t at position t which has the highest L2 error with respect to the pose reconstructed by linear interpolation at the same time index. The recursion ends once the error is below a threshold, yielding an initial set of keyposes.
- The set of keyposes is further refined by optimizing for the time indices of the keyposes and the keypose values

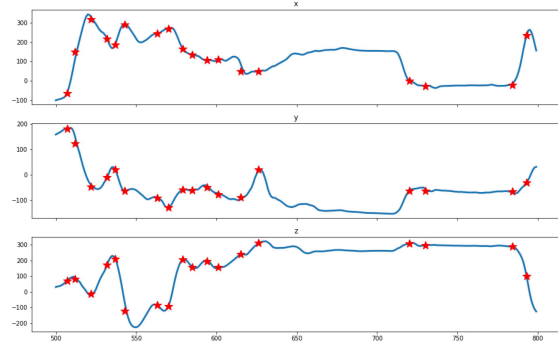


Figure 1. **Distribution of keyposes** in a short sequence. The plots depict the x, y, and z coordinates of the right wrist of subject 1 during the smoking action. We depict the locations of the keyposes as red stars. The keyposes are distributed more where the motion is the most varied and these keyposes have shorter duration.

themselves. The optimization aims to minimize the L2 error between the original sequence and the sequence reconstructed by interpolating the keyposes.

The keyposes are extracted for every training motion individually and collected in one set which is then clustered into K clusters via k-means. Each keypose is given a label determined by the cluster it is assigned to. Finally, we prune the keyposes by removing the unnecessary intermediate ones that have the same label as their preceding and succeeding keypose. An example distribution of keyposes in a sequence is shown in Figure 1.

3.2. Motion Prediction Framework

We have designed an RNN based neural network as our keypose-to-keypose prediction framework, as shown in Figure 2. The inputs to the network for step i are the tokenized keypose label L_i and the keypose duration distribution D_i discussed below. We tokenize the labels in the following steps.

1. If we know the keypose value: We compute the negative distances between the keypose value \mathbf{V}_i and all cluster centers \mathbf{C}_j , $j \in [1, C]$.
2. If we do not know the keypose value (i.e., during inference): We compute the negative distances between the keypose cluster center of label i , \mathbf{C}_{l_i} , and all cluster centers \mathbf{C}_j , $j \in [1, C]$.
3. We pass the resulting negative distances through a softmax operation with a temperature of 0.03.

Note that tokens sum up to 1 and can be thought of as a probability distribution over labels.

To obtain a duration distribution D_i , we also categorize the durations into very short (less than 4 frames), short

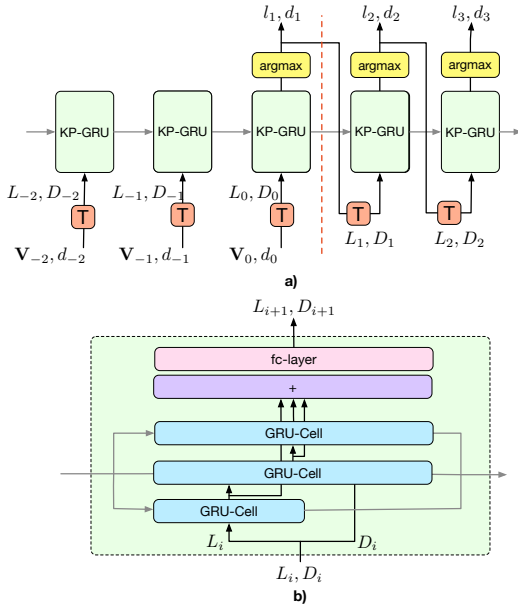


Figure 2. **Keypose-to-keypose network structure.** Figure a) depicts our overall architecture. At step i , pairs of tokenized keypose labels and durations, L_i, D_i are fed to the keypose GRU (KP-GRU) unit and the labels and durations of step $i + 1$ are predicted. The present is depicted at $i = 0$. Before this time-step, the network is given ground truth keyposes as conditioning. The tokenized label L_i is found using the keypose value \mathbf{V}_i . After time-step $i = 0$, the network is given its own predictions as input rather than the ground truth. The tokenized label L_i is found using the predicted label l_i . The orange T blocks represent the tokenization operation. Figure b) depicts the inner structure of the KP-GRU unit, which consists of a three layer GRU network followed by a fully connected layer.

(between 5 and 10 frames), medium (between 10 and 14 frames), long (between 14 and 25 frames), and very long (more than 25 frames).

The network predicts a pair of distributions: over the labels and over the duration categories. We train the network using three different loss functions:

- $E_{\text{ce-soft}}$: The cross-entropy loss between the ground-truth tokenized label and the predicted distribution over the labels to be used as a soft loss,
- $E_{\text{ce-hard}}$: The cross-entropy loss between the ground-truth label and the predicted label distribution to be used as a hard loss,
- E_{duration} : The cross-entropy loss between the predicted duration distribution and the ground-truth duration category.

The overall loss is

$$E = w_{\text{ce-soft}}E_{\text{ce-soft}} + w_{\text{ce-hard}}E_{\text{ce-hard}} + w_{\text{dur}}E_{\text{duration}}, \quad (1)$$

where $w_{\text{ce-soft}}, w_{\text{ce-hard}}, w_{\text{dur}}$ are the weights corresponding to the different loss terms.

The loss is not only enforced on the future predictions, but also on the outputs of the network as it processes the conditioning ground truth. For these past time steps, the loss is multiplied by a factor of i/I_1 , where i is the prediction step and I_1 is the number of past keyposes in the sequence. This factor is small in the beginning of the sequence, where we do not have enough past frames to base the future prediction on. As the number of past frames increases, the loss factor gets larger, until it reaches 1.

During training, the label of the next keypose l_{i+1} is determined as the one with the highest predicted probability. This label is tokenized before being fed back to the network. This procedure prevents error accumulation as the prediction progresses and guarantees that the network will never see anything very different from what it was trained on. The duration of the next keypose d_{i+1} is determined similarly: According to the category with the highest probability, the following value is set to 3 for very-short, 6 for short, 12 for medium, 16 for long, and 25 for very long.

Our network yields tokens for the keypose labels, which can be treated as probability distributions. Hence, at inference time, for each iteration of the recurrent network, we can sample the future label and duration from the predicted distributions. In practice, before sampling, we smooth the predicted distributions via a softmax with a temperature of 0.3. This sampling scheme allows us to produce multiple future sequences given a single observation.

3.3. Implementation and Training Details

We use a 3 layer GRU, depicted in Figure 2. The GRU cells all have hidden states of size 512. A Gaussian noise of magnitude 0.1 is added to the negative distances during training, to increase robustness and prevent overfitting. Furthermore, to gradually teach the network to process its own samples, we use scheduled sampling for teacher forcing, as proposed in [4]. During training, we observe 7 past keyposes and predict 12 future keyposes. At test time, we predict until we reach 5 seconds. The weights of the loss terms are set to $w_{\text{ce-hard}} = 1.0, w_{\text{ce-soft}} = 1.0, w_{\text{dur}} = 0.1$. Our network is trained for 100 epochs using a batch size of 64. We use an Adam optimizer with a learning rate of 0.0001 and a 0.01 weight decay. We report the results of the model with the highest validation score.

4. Results

4.1. Datasets

Human3.6M [17] is a standard 3D human pose dataset and has been widely used in the motion prediction literature [18, 27, 29]. It contains 15 actions performed by 7 subjects. Human pose is represented using the 3D coordi-

nates of 32 joints. As previous work [21, 26, 27], we load the exponential map representation of the dataset, remove global rotation and translation, and generate the Cartesian 3D coordinates of each joint mapped onto a uniform skeleton. Following convention, subject 5 is reserved for testing, subject 11 for validation and the remaining subjects are used for training. We test each method on the same 64 sequences formed using indices randomly selected from Subject 5’s sequences. Note that the observed keyposes are extracted using the sequence only up to the present time index as opposed to the entire sequence. The threshold used for keypose extraction is 500mm and we cluster the keyposes into 1000 clusters.

CMU-Mocap [9] is another standard benchmark dataset for motion prediction and was used in [21, 22, 27]. As explained in [22] eight action categories with enough trials are used for motion prediction. We used six out of eight actions, *basketball*, *basketball signal*, *directing traffic*, *jumping*, *soccer*, and *wash window*, as the sequences for *running and walking* were too short to provide enough input keyposes for our method. One sequence of each action is reserved for testing, one for validation and the rest are used in training. The dataset is loaded and processed in the same manner as Human3.6M. The threshold used for keypose extraction is 250mm, as some sequences are quite short, and we found that extracting more keyposes increases validation accuracy. We cluster the keyposes into 100 clusters, as this dataset is much smaller than Human3.6M and contains only 6 action classes as opposed to 15.

4.2. Baselines

We selected the following baselines for comparison purposes: HisRep [26] and TIM-GCN [21] constitute the SOTA among the methods designed for long-term prediction. For HisRep, we evaluate two versions. The first one, HisRep10, was presented as the best model in [26]. It is trained to output 10 frames and iteratively use the predicted frames as input for longer term prediction. We also evaluate HisRep125, which directly predicts 125 frames by taking 150 past frames as input. For TIM-GCN, we trained a model that observes subsequences of lengths 10, 50 and 100 and predicts 125 frames, hence tailoring the architecture to longer-term predictions of 5 seconds. Finally we compare against Mix&Match [2], and DLow [40] the SOTA methods for multiple long-term motion prediction, trained to predict 125 future frames using 100 past frames. For all baselines we used the model that gave the best validation accuracy, to be consistent with our model selection strategy.

4.3. Metrics

As in [13], we evaluate the quality and plausibility of the generated motions by passing them through an action classifier trained to predict the action category of a given

motion. If the predicted motion is plausible, such a classifier should output the correct class. To focus our evaluation on the quality of the predicted *motions*, we designed a Motion-Only Action Classifier (MOAC) based on the architecture of [23], with the pose stream removed and only the motion stream remaining. It takes as input motions encoded as the difference between poses in consecutive time-steps. This eliminates the scenario of a static prediction scoring very high under this metric. We have trained it on the training sequences of Human3.6M and CMU-Mocap separately. We report the top-K action recognition accuracy in percentages obtained with this classifier. For our method, Mix&Match, and DLow which can output multiple future predictions, we report the average accuracy over 100 predictions.

We also evaluate using the PSKL metric [33], that is, the KL divergence between the power spectrums of the ground truth future motion and predictions. As the KL divergence is asymmetric, we evaluate it in both directions and denote the results as ‘gt-pred’ and ‘pred-gt’ respectively. These values being close indicates that the ground truth and predicted motions are similarly complex.

The mean per-joint position error (MPJPE) is the most commonly used metric to evaluate motion prediction. We report the MPJPE errors at 1 second, which is the conventional long-term timestamp, and at 5 seconds. For multiple-prediction methods, we report the MPJPE results of the closest predicted sequences. We present two results: the MPJPE calculated by finding the sequence with the minimum *average* MPJPE (denoted as “ave”) and the sequence with the minimum MPJPE at the second being evaluated (denoted as “best”).

Finally, for multiple-prediction methods we report the results of a diversity metric [2, 40] for 100 predictions, calculated by finding the average pairwise L_2 distances between all pairs of generated sequences.

4.4. Comparative Results

We compare our approach to the baselines on Human3.6M and CMU-Mocap in Tables 1 and 2 on the MOAC metric. In both cases, our method outperforms the others by a large margin. In Table 3, we report the results for the PSKL metric and show that we outperform the other methods by having both lower PSKL values and having very close ‘gt-pred’ and ‘pred-gt’ values.

In Table 4, we evaluate the diversity and MPJPE losses of the predicted sequences. We observe that the diversity value of our method increases as we increase the softmax temperature used for sampling during inference. Increased diversity allows us to achieve lower MPJPE values since we now have a higher chance of sampling the correct future motion. However this also leads to a drop in average MOAC accuracies. Therefore, in our evaluations we choose to set this value to 0.3, trading a bit of accuracy for more diverse

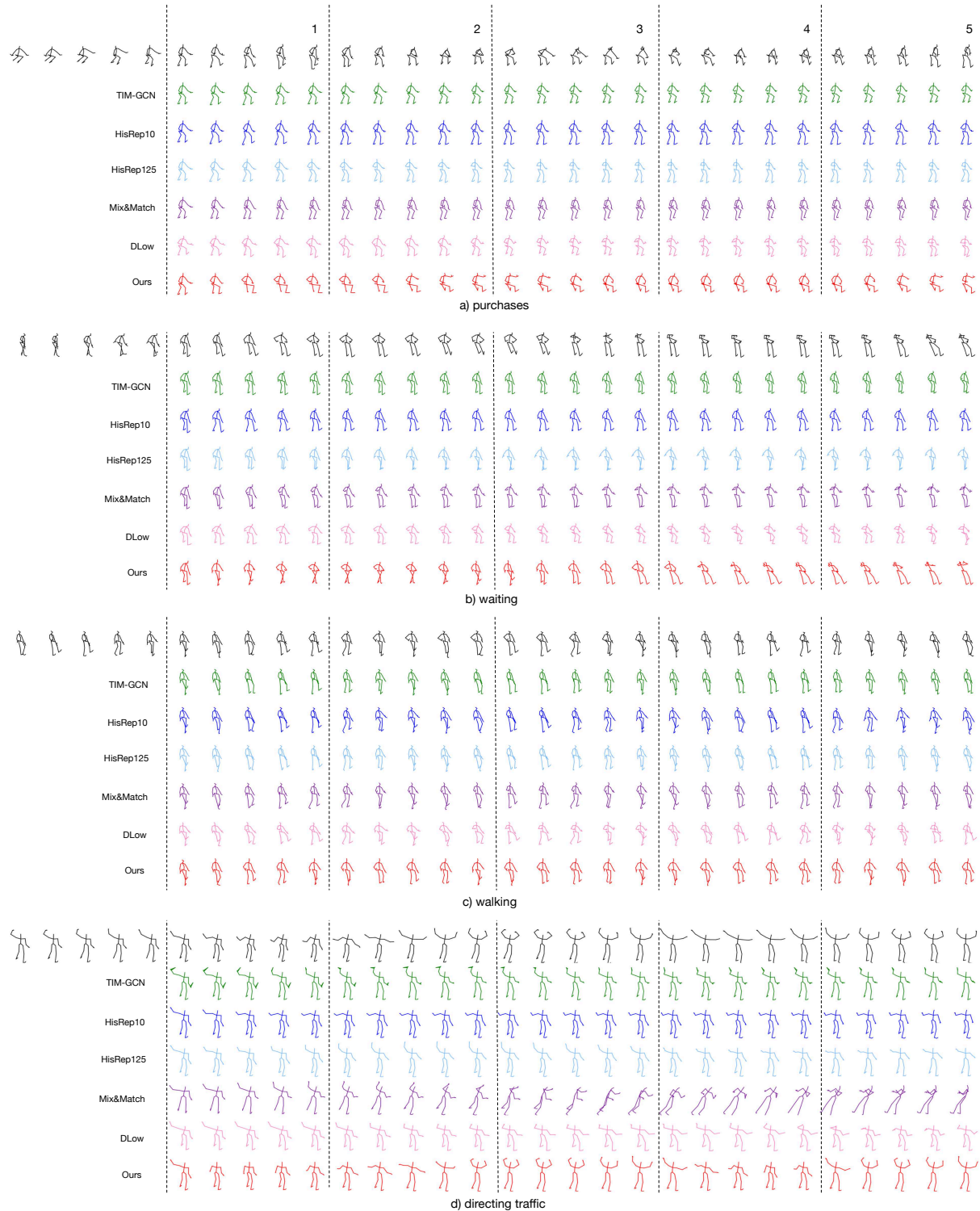


Figure 3. **Qualitative evaluation of our results** on the Human3.6M (Figures a, b, c) and CMU-Mocap (Figure d) datasets. We present the results of: TIM-GCN (green), HisRep10 (dark blue), HisRep125 (light blue), Mix&Match (violet), DLow (pink), Ours (red). For the multiple prediction methods we display the prediction that has the lowest average MPJPE error with respect to the ground truth. The top black row depicts the ground truth, and the first 5 poses are the conditioning ground truth. The numbers at the top indicate the future timestamp in seconds. We produce more dynamic poses for purchases, waiting, and directing traffic which are acyclic motions. For cyclic motions such as walking, the other methods are also able to produce dynamic poses.

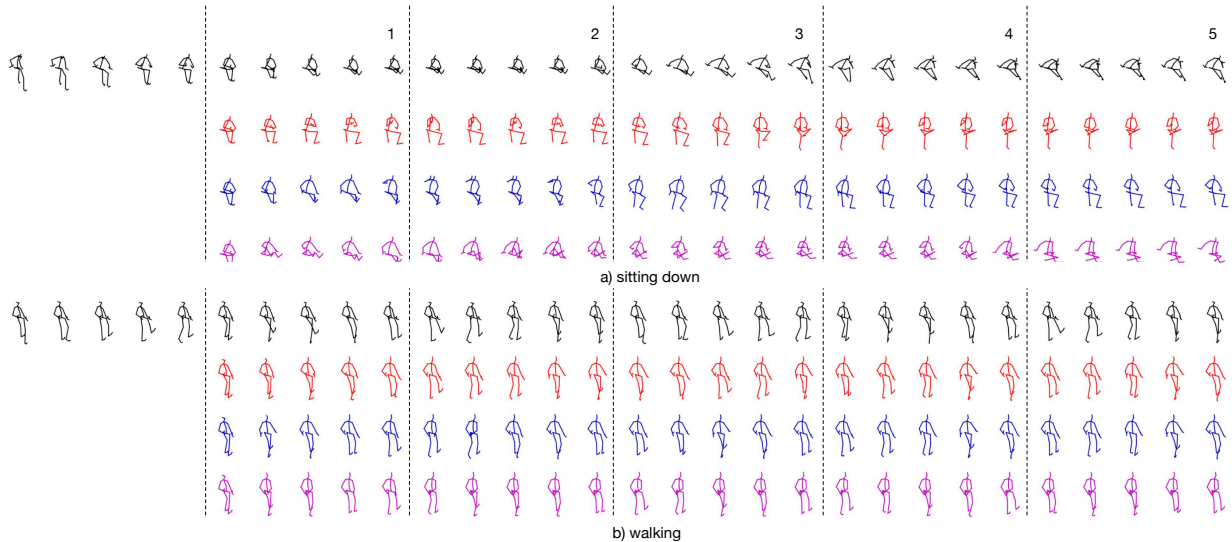


Figure 4. **Qualitative results of our multiple motion prediction** obtained by sampling the predicted label distribution. The numbers at the top indicate the future timestamp in seconds. The top row in black depicts the ground truth, and the remaining rows in color are our generated motions. The sampled motions are diverse, yet can all still be classified as “sitting down” and “walking”.

	top-1	top-2	top-3	top-5
oracle	51	70	79	91
TIM-GCN	16	26	36	55
HisRep10	21	32	39	53
HisRep125	20	32	44	60
Mix&Match	18	32	45	61
DLow	16	26	39	56
Ours	32	44	55	69

Table 1. **Results of the motion-only action classifier (MOAC) on the Human3.6M dataset.** We compare the classification accuracies of the motion predicted via our work compared to SOTA methods. We also report the accuracies of the oracle, which evaluates ground truth future motions, as an upper bound. We report the top-1, top-2, top-3 and top-5 accuracies. The results indicate that the motion predicted by our keypose network is more realistic than the motion predicted by the competing methods.

	top-1	top-2	top-3	top-5
oracle	86	88	90	100
TIM-GCN	44	69	85	95
HisRep10	42	54	62	88
HisRep125	34	48	57	82
Mix&Match	30	39	58	85
DLow	36	49	60	79
Ours	75	83	96	100

Table 2. **Results of the motion-only action classifier (MOAC) on the CMU-Mocap dataset.** We compare the MOAC accuracies of our method to SOTA methods. We observe that the trend is similar to H36M, as we achieve higher accuracies than SOTA methods.

predictions. Our method outperforms the others in having both high diversity, the best average MOAC accuracies, and low MPJPE. For MPJPE, at 1 second we are comparable to

the other methods, but at 5 seconds, especially for the “best” MPJPE, our performance is noticeably better.

Fig. 3 depicts qualitative results for the purchases, waiting and walking actions of Human3.6M and the directing traffic action of CMU-Mocap. Close visual inspection reveals that, while all methods work reasonably well on cyclic motions such as walking, ours does better on the acyclic ones, such as purchases. It produces wider motion ranges than the others that tend to predict less dynamic motions. Fig. 4 depicts qualitative results for multiple predictions. Our method is capable of generating diverse, yet still plausible motions.

4.5. Ablation Study on Keypose Retrieval Methods

We evaluate the effect of using keyposes obtained via different strategies: sampling, clustering and ours. The naive-sampling method evenly samples the motion at a rate of 15 frames, which is the average keypose duration from our method. The keyposes are then clustered without any keypose pruning. This method also doesn’t require predicting durations, as the duration will always be 15. We also evaluate naive-sampling-pruned, where the keyposes are found through naive sampling, and then pruned. The clustering method performs clustering on *every* pose in the sequence, rather than only on the poses found via our optimization strategy and pruned afterwards.

As shown in Table 5, our keypose method achieves the highest MOAC accuracies. The comparison with the naive-sampling method emphasizes the importance of having variable-duration keyposes, as opposed to evenly sampling the motion. The comparison with the clustering method emphasizes the importance of optimizing for the keyposes.

	Human3.6M				CMU-MoCap			
	gt-pred	pred-gt	average	difference	gt-pred	pred-gt	average	difference
TIM-GCN	0.0069	0.0098	0.0083	0.0029	0.0073	0.0101	0.0087	0.0028
HisRep10	0.0076	0.0129	0.0103	0.0053	0.0061	0.0081	0.0071	0.0020
HisRep125	0.0070	0.0097	0.0083	0.0027	0.0065	0.0093	0.0079	0.0028
Mix&Match	0.0067	0.0075	0.0071	0.0008	0.0090	0.0104	0.0097	0.0014
DLow	0.0080	0.0062	0.0071	0.0008	0.0069	0.0073	0.0071	0.0008
Ours	0.0062	0.0060	0.0061	0.0002	0.0060	0.0057	0.0058	0.0003

Table 3. **Results on the PSKL metric** on both the Human3.6M and CMU-MoCap datasets, lower numbers indicate better results. We report the PSKL results between ground truth and predictions (‘gt-pred’), predictions and ground truth (‘pred-gt’), their averages, and the absolute difference between them. For the multiple prediction methods, Mix&Match and Ours, we report the best PSKL value which are the results of prediction that had the most similar power spectrum to the ground truth future motion. We observe that the trend is similar to the MOAC results and our method outperforms the SOTA.

	div	acc	1s ave	1s best	5s ave	5s best
TIM	-	16	143	143	196	196
HisRep10	-	21	116	116	197	197
HisRep125	-	20	136	136	191	191
Mix&Match	1002	18	161	156	244	237
DLow	3501	16	136	131	189	171
Ours (0.1)	6662	33	179	171	208	175
Ours (0.3)	10474	32	158	143	197	150
Ours (0.5)	12210	31	149	129	192	139
Ours (0.7)	13385	29	146	121	190	131
Ours (1.0)	14924	22	146	117	195	123

Table 4. **Results on the diversity metric, top-1 MOAC accuracy and MPJPE errors** on the Human3.6 dataset. Higher diversity values indicate more variation in the multiple future predictions and lower MPJPE values indicate closer predictions to ground truth future motion. We have highlighted close best results in bold. We provide several results of our method with varying sampling softmax temperature, indicated in parentheses. As the temperature increases, the diversity values of the predictions increase and MPJPE values decrease, however the average top-1 MOAC accuracy begins to decrease as well.

	top-1	top-2	top-3	top-5
Naive-sampling	28	38	51	67
Naive-sampling-pruned	30	42	52	63
Clustering	24	37	48	66
Ours	32	44	55	69

Table 5. **Analysis on the method of obtaining keyposes.** We compare the MOAC accuracies of different keypose methods: naive-sampling, naive-sampling-pruned, clustering and ours. The method we currently use achieves higher classification accuracies than the other two methods, indicating that the quality of the keyposes affects the performance.

Further ablation studies on the training strategies and the number of clusters are provided in the supplementary material.

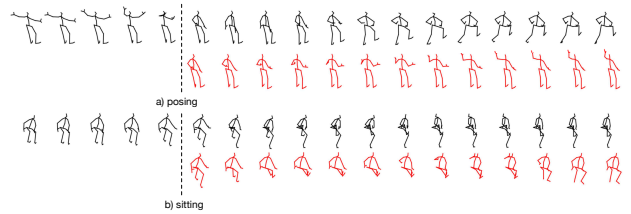


Figure 5. **Examples of failure** to predict the correct keypose labels. The top example is from the category ‘‘posing’’, however once our model detects the extended arms, it switches to the waving motion resembling the poses from the ‘‘greeting’’ category. The bottom example is from the category ‘‘sitting’’. Though the motion of the legs are plausible, our prediction lifts a hand to its head, resembling a motion from the ‘‘phoning’’ category.

4.6. Limitations and Failure Modes

The main failure mode of our approach arises from incorrect cluster label prediction, as illustrated in Figure 5, and from the fact that, while powerful, cluster centers cannot perfectly model all poses. To overcome this, we will study in future work the use of other clustering strategies such as the deep-learning based one of [38] that can be incorporated into our architecture for end-to-end training.

5. Conclusion

To the best of our knowledge, our work constitutes the first attempt to predict diverse futures for long-term durations of 5 seconds. Our method is built on predicting pairs of keypose labels and durations. Using these, we reconstruct the motion via linear interpolation. To evaluate our results, we have introduced a new action classifier, MOAC, that specifically focuses on the transitions between poses, thus placing an emphasis on the correctness of *motion*, rather than that of *poses*. Our experiments have evidenced that our method yields more dynamic and realistic poses than the recent SOTA work, even when tailored to learn patterns for long term prediction. Furthermore, our approach lets us easily sample diverse future motions.

References

- [1] V. Adeli, E. Adeli, I. Reid, J.C. Niebles, and H. Rezatofighi. Socially and Contextually Aware Human Motion and Pose Forecasting. In *International Conference on Intelligent Robots and Systems*, 2020. 2
- [2] S. Aliakbarian, F. S. Saleh, M. Salzmann, L. Petersson, and S. Gould. A Stochastic Conditioning Scheme for Diverse Human Motion Prediction. In *Conference on Computer Vision and Pattern Recognition*, 2020. 2, 5, 12
- [3] E. Barsoum, J. Kender, and Z. Liu. HP-GAN: Probabilistic 3D Human Motion Prediction via GAN. In *Conference on Computer Vision and Pattern Recognition*, 2017. 2
- [4] S. Bengio, O. Vinyals, N. Jaitly, and N. Shazeer. Scheduled Sampling for Sequence Prediction with Recurrent Neural Networks. In *Advances in Neural Information Processing Systems*, 2015. 4, 10
- [5] Victoria Bloom, Vasileios Argyriou, and Dimitrios Makris. Linear latent low dimensional space for online early action recognition and prediction. *Pattern Recognition*, 72:532–547, 2017. 2
- [6] J. Butepage, M.J. Black, D. Kragic, and H. Kjellstrom. Deep Representation Learning for Human Motion Prediction and Classification. In *Conference on Computer Vision and Pattern Recognition*, 2017. 2
- [7] Judith Bütepage, Hedvig Kjellström, and Danica Kragic. Anticipating Many Futures: Online Human Motion Prediction and Generation for Human-Robot Interaction. In *International Conference on Robotics and Automation*, 2018. 1, 2
- [8] J. Bütepage, H. Kjellström, and D. Kragic. Predicting the What and How - A Probabilistic Semi-Supervised Approach to Multi-Task Human Activity Modeling. In *Conference on Computer Vision and Pattern Recognition*, pages 2923–2926, 2019. 2
- [9] CMU Graphics Lab Motion Capture Database, 2010. <http://mocap.cs.cmu.edu/>. 5
- [10] E. Corona, A. Pumarola, G. Alenyà, and F. Moreno-Noguer. *Context-Aware Human Motion Prediction*. 2020. 2
- [11] J. Fan, X. Shen, and Y. Wu. Scribble Tracker: A Matting-Based Approach for Robust Tracking. *IEEE Transactions on Pattern Analysis and Machine Intelligence*, 34:1633–1644, 2012. 1
- [12] K. Fragkiadaki, S. Levine, P. Felsen, and J. Malik. Recurrent Network Models for Human Dynamics. In *International Conference on Computer Vision*, 2015. 2
- [13] P. Ghosh, J. Song, E. Aksan, and O. Hilliges. Learning Human Motion Models for Long-Term Predictions. In *International Conference on 3D Vision*, 2017. 1, 2, 5
- [14] L. Gui, K. Zhang, Y. Wang, X. Liang, J. M. F. Moura, and M. Veloso. Teaching robots to predict human motion. In *International Conference on Intelligent Robots and Systems*, 2018. 1
- [15] Chuan Guo, Xinxin Zuo, Sen Wang, Shihao Zou, Qingyao Sun, Annan Deng, Minglun Gong, and Li Cheng. Action2motion: Conditioned generation of 3d human motions. In *Proceedings of the 28th ACM International Conference on Multimedia (MM '20)*, 2020. 2
- [16] G. Habibi, N. Jaipuria, and J. P. How. Context-Aware Pedestrian Motion Prediction in Urban Intersections. In *arXiv Preprint*, 2018. 1
- [17] C. Ionescu, I. Papava, V. Olaru, and C. Sminchisescu. Human3.6M: Large Scale Datasets and Predictive Methods for 3D Human Sensing in Natural Environments. *IEEE Transactions on Pattern Analysis and Machine Intelligence*, 2014. 4
- [18] A. Jain, A.R. Zamir, and S. Savaresea A. adn Saxena. Structural-Rnn: Deep Learning on Spatio-Temporal Graphs. In *Conference on Computer Vision and Pattern Recognition*, 2016. 2, 4
- [19] S. Kiciroglu, H. Rhodin, S. Sinha, M. Salzmann, and P. Fua. Activemocap: Optimized Viewpoint Selection for Active Human Motion Capture. In *Conference on Computer Vision and Pattern Recognition*, 2020. 1
- [20] L. Kovar, M. Gleicher, and F. Pighin. Motion Graphs. In *ACM SIGGRAPH*, pages 473–482, July 2002. 2
- [21] T. Lebailly, S. Kiciroglu, M. Salzmann, P. Fua, and W. Wang. Motion Prediction Using Temporal Inception Module. In *Asian Conference on Computer Vision*, 2020. 1, 2, 3, 5, 12
- [22] M. Li, S. Chen, Y. Zhao, Y. Zhang, Y. Wang, and Q. Tian. Dynamic Multiscale Graph Neural Networks for 3D Skeleton Based Human Motion Prediction. In *Conference on Computer Vision and Pattern Recognition*, June 2020. 2, 5
- [23] Y. Li, L. Yuan, and N. Vasconcelos. Co-Occurrence Feature Learning from Skeleton Data for Action Recognition and Detection with Hierarchical Aggregation. In *International Joint Conference on Artificial Intelligence*, 2018. 5, 12, 13
- [24] Li Liu, Ling Shao, Xiantong Zhen, and Xuelong Li. Learning discriminative key poses for action recognition. *IEEE Transactions on Cybernetics*, 43(6):1860–1870, 2013. 2
- [25] F. Lv and R. Nevatia. Single View Human Action Recognition Using Key Pose Matching and Viterbi Path Searching. In *Conference on Computer Vision and Pattern Recognition*, pages 1–8, 2007. 2
- [26] W. Mao, M. Liu, and M. Salzmann. History Repeats Itself: Human Motion Prediction via Motion Attention. In *European Conference on Computer Vision*, 2020. 1, 2, 3, 5, 12
- [27] W. Mao, M. Liu, M. Salzmann, and H. Li. Learning Trajectory Dependencies for Human Motion Prediction. In *International Conference on Computer Vision*, 2019. 1, 2, 3, 4, 5
- [28] J. Martinez, M.J. Black, and J. Romero. On Human Motion Prediction Using Recurrent Neural Networks. In *Conference on Computer Vision and Pattern Recognition*, 2017. 1, 2
- [29] J. Martinez, R. Hossain, J. Romero, and J.J. Little. A Simple Yet Effective Baseline for 3D Human Pose Estimation. In *International Conference on Computer Vision*, 2017. 4
- [30] R. Morais, V. Le, T. Tran, B. Saha, M. Mansour, and S. Venkatesh. Learning Regularity in Skeleton Trajectories for Anomaly Detection in Videos. In *Conference on Computer Vision and Pattern Recognition*, 2019. 1
- [31] D. Pavllo, D. Grangier, and M. Auli. Quaternet: A Quaternion-Based Recurrent Model for Human Motion. In *British Machine Vision Conference*, 2018. 3

- [32] Mathis Petrovich, Michael J. Black, and Gül Varol. Action-conditioned 3D human motion synthesis with transformer VAE. In *International Conference on Computer Vision*, pages 10985–10995, Oct. 2021. 2
- [33] A. H. Ruiz, J. Gall, and F. Moreno-Noguer. Human Motion Prediction via Spatio-Temporal Inpainting. In *International Conference on Computer Vision*, 2019. 5
- [34] L. Shi, L. Wang, C. Long, S. Zhou, M. Zhou, Z. Niu, and G. Hua. Sparse graph convolution network for pedestrian trajectory prediction. In *Conference on Computer Vision and Pattern Recognition*, 2021. 1
- [35] Ian Simon and Sageev Oore. Performance rnn: Generating music with expressive timing and dynamics, 2017. 2
- [36] Bob Sturm, João Santos, Oded Ben-Tal, and Iryna Korshunova. Music transcription modelling and composition using deep learning. *Conference on Computer Simulation of Musical Creativity*, 04 2016. 2
- [37] S. Tang, M. Golparvar-Fard, M. Naphade, and M. Gopalakrishna. Video-Based Motion Trajectory Forecasting Method for Proactive Construction Safety Monitoring Systems. *Journal of Computing in Civil Engineering*, 34:04020041, 11 2020. 1
- [38] A. van den Oord, O. Vinyals, and K. Kavukcuoglu. Neural discrete representation learning. In *Advances in Neural Information Processing Systems*, volume 30, 2017. 8
- [39] B. Wang, E. Adeli, H.-K. Chiu, D.-A. Huang, and J. C. Niebles. Imitation Learning for Human Pose Prediction. In *International Conference on Computer Vision*, pages 7123–7132, 2019. 2
- [40] Ye Yuan and Kris Kitani. Dlow: Diversifying latent flows for diverse human motion prediction. In *European Conference on Computer Vision*, 2020. 2, 5, 12
- [41] J. Zhang and C. Zong. Deep neural networks in machine translation: An overview. *IEEE Intelligent Systems*, 30(5), 2015. 2

6. Ablation Studies

In our ablation studies, we report the MOAC accuracy results on the validation set as well as the test set. The validation accuracy reported is the sum of top-1, top-2, top-3 and top-5 OMAC accuracies on the validation set. For all cases, we chose our final model as the one obtaining the highest validation accuracy. Please note that the results presented here are the not the average accuracies of multiple predicted motions. In order to evaluate quickly, we chose to predict a single future in a “greedy” manner: instead of sampling multiple futures from the predicted cluster probability distribution, we simply choose the one with the highest probability. We then report the average accuracies of these single predictions.

Number of clusters We report results of using different number of clusters in Table 6. Using too many or too few clusters leads to both lower validation and test accuracies.

We also note that using more clusters leads to higher training time. We chose to use 1000 clusters in our final model.

Keypose Error Threshold The first step of the keypose extraction algorithm recursively selects keyposes from the sequence until the reconstruction error is below a threshold. In our experiments, we chose this number to be 500. We report results of using different error thresholds in extracting keyposes in Table 7. Using a threshold that is too low or high leads to lower validation accuracies. We also note that using a higher threshold leads to sparser keyposes, leading to a smaller training set. This allows for faster training, however the accuracy drops significantly when this threshold is set too high.

Scheduled Sampling For scheduled sampling, we use inverse sigmoid decay,

$$\epsilon_i = k / (k + \exp(i/k)) \quad (2)$$

as presented in [4] where k is the hyper-parameter of scheduled sampling and ϵ_i is the probability that teacher forcing is performed in that iteration. Table 8 reports the results of using scheduled sampling for teacher forcing with varying k . We conclude that using scheduled sampling with $k = 10$ gives the highest accuracies.

Training Softmax Heat During training, we tokenize our keyposes by passing the inverse distances of the keypose value to the cluster centers through a heated softmax function. In Table 9, we conduct an ablation study on the value of the heat. We observe that too much heat and too little heat both lead to low validation and test accuracies. In our experiments we set the softmax heat for training to 0.03.

Past Supervision In Table 10, we analyze whether enforcing the loss on the outputs of the network as it processes the conditioning ground truth increases accuracy. We observe that this training strategy indeed increases both validation and test accuracies.

Hidden Layer Size Table 11 reports the results of using different hidden layer sizes. We choose 512 as it leads to higher accuracies.

Noise During training, we add noise to the inverse distances as a part of the keypose tokenization. In Table 12 we analyze the effects of this noise. We find that, indeed, adding a noise with standard deviation 0.1 is useful and increases accuracies.

	top-1	top-2	top-3	top-5	val-acc	training-time (hours)
100	24	37	47	66	2.45	1.36
250	28	41	51	68	2.48	1.54
500	30	42	52	69	2.58	1.78
1000 (Ours)	32	45	54	69	2.60	1.99
2000	32	43	52	69	2.52	2.23
3000	29	38	47	65	2.29	2.65

Table 6. **Ablation study on number of cluster centers** We observe that we have similar performance around using 1000 clusters, with 1000 giving the highest accuracy. As the number of clusters decreases, the training-time also decreases but the accuracy drops. This is caused by the final layer of the keypose network being a fully connected one, going from the hidden layer size (512) to the number of clusters. A decrease in the number of clusters therefore leads to a smaller network which is faster to train. An increased number of clusters also results in a drop of accuracy and also an increase in training-time.

	top-1	top-2	top-3	top-5	val-acc	training set size	training-time (hours)
300	29	38	49	66	2.48	12286	2.45
500 (Ours)	32	45	54	69	2.60	8760	1.99
750	32	41	51	66	2.50	5403	1.39
1000	32	42	50	64	2.28	3036	1.16

Table 7. **Ablation study on the error threshold for the keypose extraction algorithm.** We observe that we have similar performance around using 500 as the error threshold, with 500 giving the highest accuracy. As the error threshold decreases, the training-time increases because the size of the training set increases. As the error threshold increases, the training-time decreases as the set of keyposes becomes sparser. However the accuracy drops dramatically.

	top-1	top-2	top-3	top-5	val-acc
No-tf	30	43	53	67	2.49
Always-tf	31	42	53	70	2.49
$k = 10$ (Ours)	32	45	54	69	2.60
$k = 20$	33	43	54	69	2.54
$k = 60$	31	40	50	68	2.38
$k = 100$	32	40	49	66	2.38

Table 8. **Ablation study on the scheduled sampling** used for determining the probability of teacher forcing. We first evaluate the cases of not using scheduled sampling at all: either by not using teacher forcing at all during training (first row), or always using teacher forcing during training (second row). We then evaluate different cases of using scheduled sampling by varying the scheduled-sampling hyperparameter k . We observe that using scheduled sampling and setting the parameter k to 10 gives the best results in terms of validation accuracy, but the test accuracies are very close in general.

	top-1	top-2	top-3	top-5	val-acc
heat = 0.01	28	41	49	69	2.44
heat = 0.02	30	42	50	70	2.51
heat = 0.03 (Ours)	32	45	54	69	2.60
heat = 0.04	33	43	52	68	2.58
heat = 0.07	29	40	50	68	2.57
heat = 0.1	30	41	52	68	2.54
heat = 1.0	24	35	45	63	1.94

Table 9. **Ablation study on the heat used during the heated softmax** operation of the label tokenization. We use the heat 03 during training as it gives the highest validation accuracy, which also corresponds to the highest test accuracies. We observe that when the heat is too small or too large, the validation accuracy drops significantly.

Weights of loss functions Table 13 reports the results of using different weights for the three loss functions we use.

We find that setting these weights to $w_{ce-soft} = w_{ce-hard} =$

	top-1	top-2	top-3	top-5	val-acc
No-past-supervision	32	43	53	69	2.55
With-past-supervision (Ours)	32	45	54	69	2.60

Table 10. **Ablation study on supervising already seen keyposes.** We observe that supervising on the conditioning past also improves validation and test accuracies.

	top-1	top-2	top-3	top-5	val-acc
hidden size = 256	31	41	52	68	2.52
hidden size = 512 (Ours)	32	45	54	69	2.60
hidden size = 1024	32	42	51	66	2.59

Table 11. **Ablation study on the hidden layer size of the GRU cells.** We observe that using 512 as the hidden layer size leads to higher accuracies.

	top-1	top-2	top-3	top-5	val-acc
no-noise	28	38	47	60	2.31
noise = 0.05	31	42	52	67	2.51
noise = 0.1 (Ours)	32	45	54	69	2.60
noise = 0.5	19	32	41	58	2.48
noise = 1.0	14	23	34	53	1.48

Table 12. **Ablation study on the standard deviation of the Gaussian noise** added to the inverse distances during keypose tokenization. We observe that adding a noise of 1 increases accuracies, while using too much or too little noise leads to worse results.

	$w_{\text{duration}} = 0.1$					$w_{\text{duration}} = 1.0$				
	top-1	top-2	top-3	top-5	val-acc	top-1	top-2	top-3	top-5	val-acc
$w_{\text{ce-soft}} = 0, w_{\text{ce-hard}} = 1.0$	32	42	52	68	2.54	32	43	55	69	2.54
$w_{\text{ce-soft}} = 0.1, w_{\text{ce-hard}} = 1.0$	33	43	55	71	2.56	31	43	54	70	2.55
$w_{\text{ce-soft}} = w_{\text{ce-hard}} = 1.0$	32	45	54	69	2.60	32	43	54	70	2.57
$w_{\text{ce-soft}} = 1.0, w_{\text{ce-hard}} = 0.1$	32	41	52	67	2.56	33	44	55	70	2.55
$w_{\text{ce-soft}} = 1.0, w_{\text{ce-hard}} = 0$	32	42	53	68	2.54	31	43	54	70	2.55

Table 13. **Ablation study on the weights of different loss functions we use during training.** In the end, we chose the weight proportions of $w_{\text{ce-soft}} = w_{\text{ce-hard}} = 1.0, w_{\text{duration}} = 0.1$ as this gave the highest validation accuracy.

1.0 and $w_{\text{duration}} = 0.1$ leads to the highest accuracies.

7. Training-Time Analysis

We compare the training time of different methods in Table 14. We trained the methods of TIM-GCN [21] and HisRep [26] for 50 epochs, Mix&Match [2] for 100k iterations, and DLow [40] for 500 epochs each for both training steps, as recommended in their papers. We observe that our method is the fastest, with TIM-GCN also being relatively quick to train compared to the other methods.

8. Full Action Classifier

Model In order to run a complete analysis, we report the results on a full action classifier (FAC). The full action classifier is based fully on [23]. As opposed to the only-motion action classifier (OMAC), it also processed the poses in a

	training-time (hours)
TIM-GCN	2.9
HisRep10	11.2
HisRep125	23.5
Mix&Match	14.8
DLow	30.9
Ours	2.0

Table 14. **Training-time of different methods.** Our method is the fastest to train among state of the art motion prediction methods.

separate stream. The two architectures are depicted in Figure 6.

Results on FAC Metric We report the results of FAC on Human3.6M in Table 15. We note the high performance of

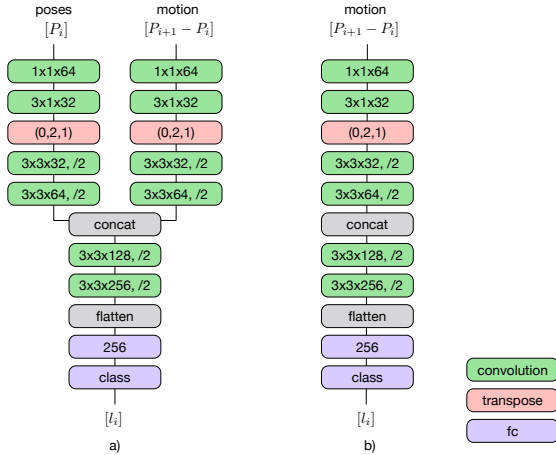


Figure 6. **Action classifier architectures** based on [23]. a) Full action classifier (FAC), which takes as input both the poses and the motion (difference between consecutive poses). b) Motion-only action classifier (MOAC), which takes only motion as input.

the mean-pose predictor on this metric. This predictor produces a sequence consisting of a single pose, which is set to the mean pose of the action category. The mean poses of the action categories were found using the training set. Despite having no motion whatsoever, this predictor is able to outperform everyone, except for the oracle, which evaluates the ground truth future motion. We also point out that the static predictor, which predicts a sequence consisting only of the last-seen pose, also does relatively well on this metric. This predictor also produces no motion whatsoever.

While HisRep125 performs best out of the prediction methods, it had a much lower MOAC performance compared to our method. This indicates that the motions we predict are more realistic than the ones HisRep125 produces but that the FAC classifier can use a few well-predicted static poses to guess the motion nevertheless.

We also report the results of FAC on CMU Mocap Dataset in Table 16. The trend is similar to the results on Human3.6M, with the extremely high performance of the mean-pose predictor. This further leads us to conclude that this metric is able to distinguish sequences which have no motion at all, therefore not being a reliable metric for our purposes.

Training Details The action recognition models are trained to classify sequences of 125 frames (5 seconds). Both models are trained with Adam optimizer, using a learning rate of $1e - 5$, and weight decay of $1e - 4$. In order to make the model more robust to overfitting, we have added Gaussian noise during training to the input data. With independent probabilities of 0.5, a noise of 20 mm standard deviation is added to the motion and noise of 30 mm stan-

	top-1	top-2	top-3	top-5
Oracle	59	78	86	94
Mean-Pose	53	67	73	80
Static	28	40	51	64
TIM-GCN	39	52	63	76
HisRep10	36	53	63	76
HisRep125	42	56	67	80
Mix&Match	29	45	58	71
DLow	23	46	54	65
Ours	39	53	61	74

Table 15. **Results of the full action classifier (FAC) on the Human3.6M dataset.** We compare the classification accuracies of the motion predicted via our work compared to SOTA methods. The oracle evaluates ground truth future motions. Static evaluates a sequence consisting of only the last seen pose, i.e. not predicting any motion at all. Its relatively high performance despite being severely handicapped indicates that this is not a very reliable metric. Mean-pose evaluates a sequence consisting of a static pose set to the mean pose of the action category and is able to achieve results higher than everyone, emphasizing how little importance motion carries for this metric.

	top-1	top-2	top-3	top-5
Oracle	76	94	100	100
Mean-Pose	100	100	100	100
Static	72	80	95	100
TIM-GCN	73	85	95	100
HisRep10	71	90	98	100
HisRep125	74	85	92	100
Mix&Match	44	51	66	94
Dlow	57	62	64	92
Ours	74	76	89	93

Table 16. **Results of the full action classifier (FAC) on the CMU-Mocap Dataset.** The trend is similar to the results on Human3.6M. In this case, it is even more striking that the Mean-Pose predictor is able to get 100% accuracy on even top-1, with using just a single static pose. Static, which evaluates a sequence consisting of only the last seen pose also has a high performance rivalling the results of the learning-based prediction methods.

dard deviation is added to the poses. We have found that this procedure improves the validation accuracies. The trained models and the training code will also be released by us upon acceptance.

9. Cluster center visualization

We show a sample of 500 keypose cluster centers in Figure 7. It is necessary for them to be varied in order to be able to express the wide range of poses seen across different action categories. We find that the keypose cluster centers include poses from many categories, such as sitting, crouch-

ing, squatting, standing, walking, and making different arm gestures.

10. Additional Qualitative Results

Additional qualitative results on the Human3.6M dataset can be seen in Figures 8,9,10. The top row in black depicts the ground truth poses and the first five poses represent the last seen 1 second of the conditioning ground truth. We display the action categories which we were unable to show in our main paper due to lack of space. We again draw attention to the wide gestures our model is able to generate and the overall dynamism of the predicted motions as compared to the SOTA methods.

Qualitative results for the CMU-Mocap dataset can be seen in Figures 11,12. We see that we achieve more dynamic and realistic poses on this dataset as well.

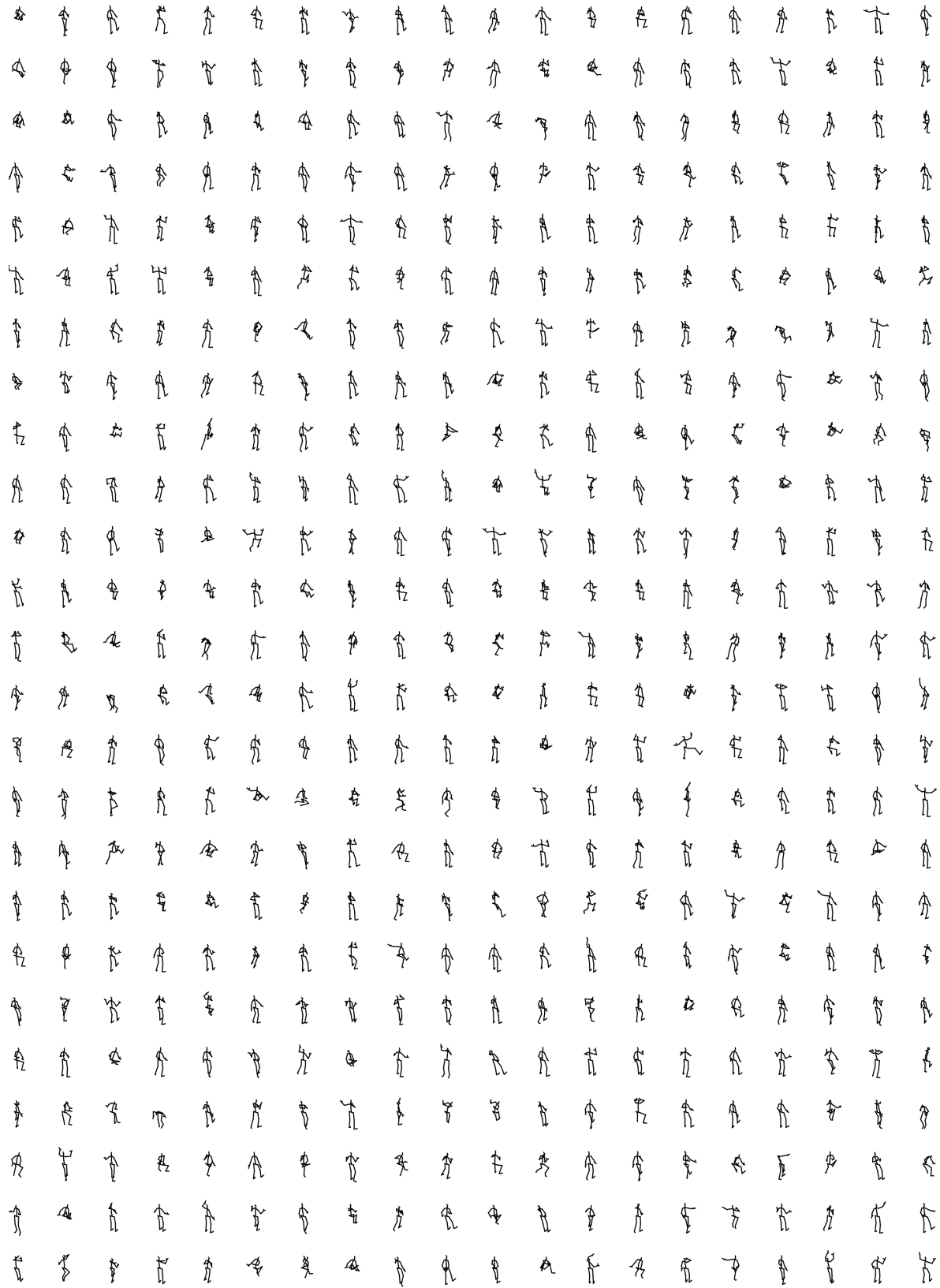


Figure 7. **Visualization of keypose cluster centers.** The sampled 500 keypose cluster centers here show that the cluster centers are quite varied and are able to represent the keyposes throughout the different categories of motions.

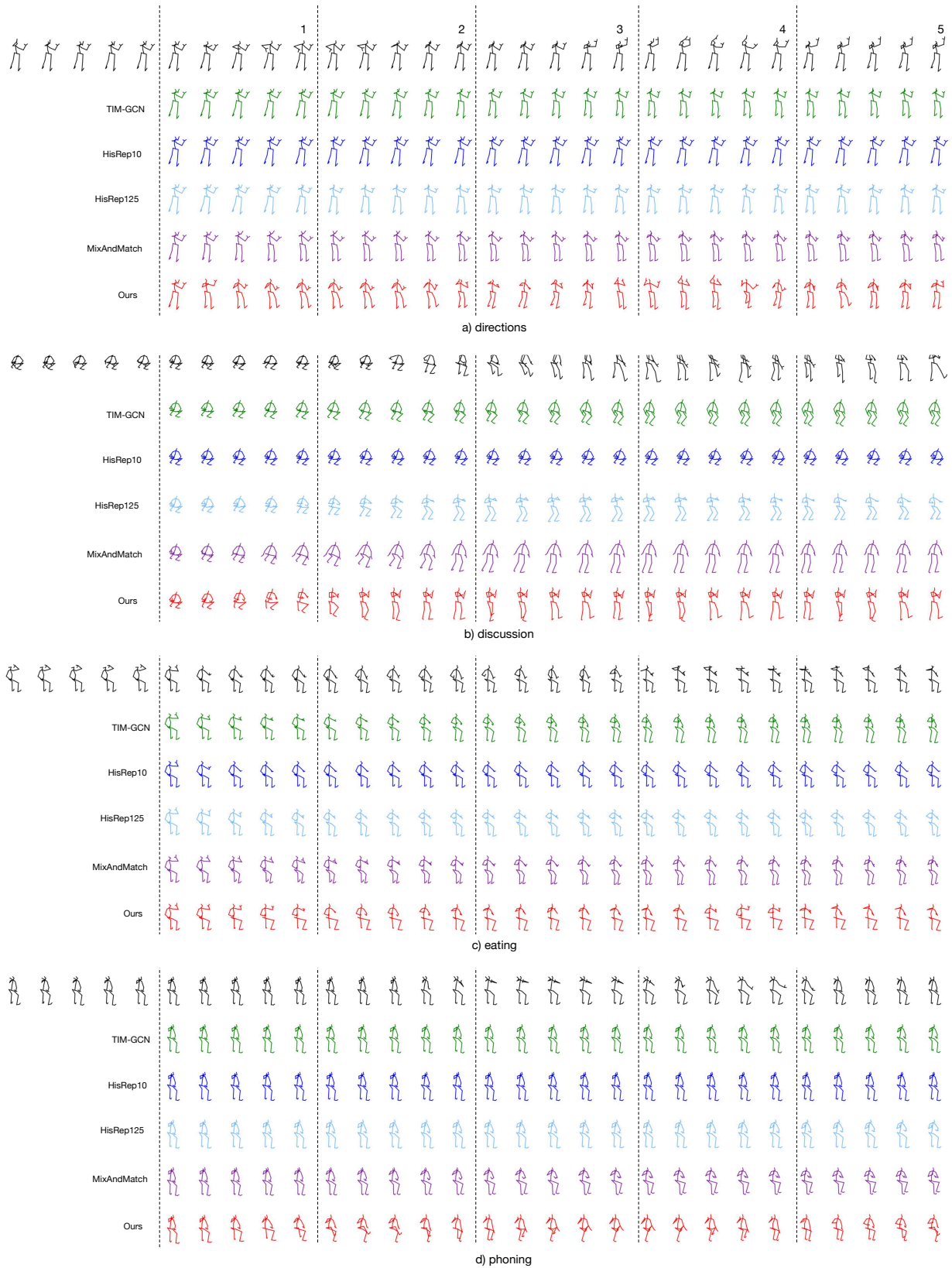


Figure 8. Qualitative results on Human3.6M of actions "directions", "discussion", "eating", "phoning".

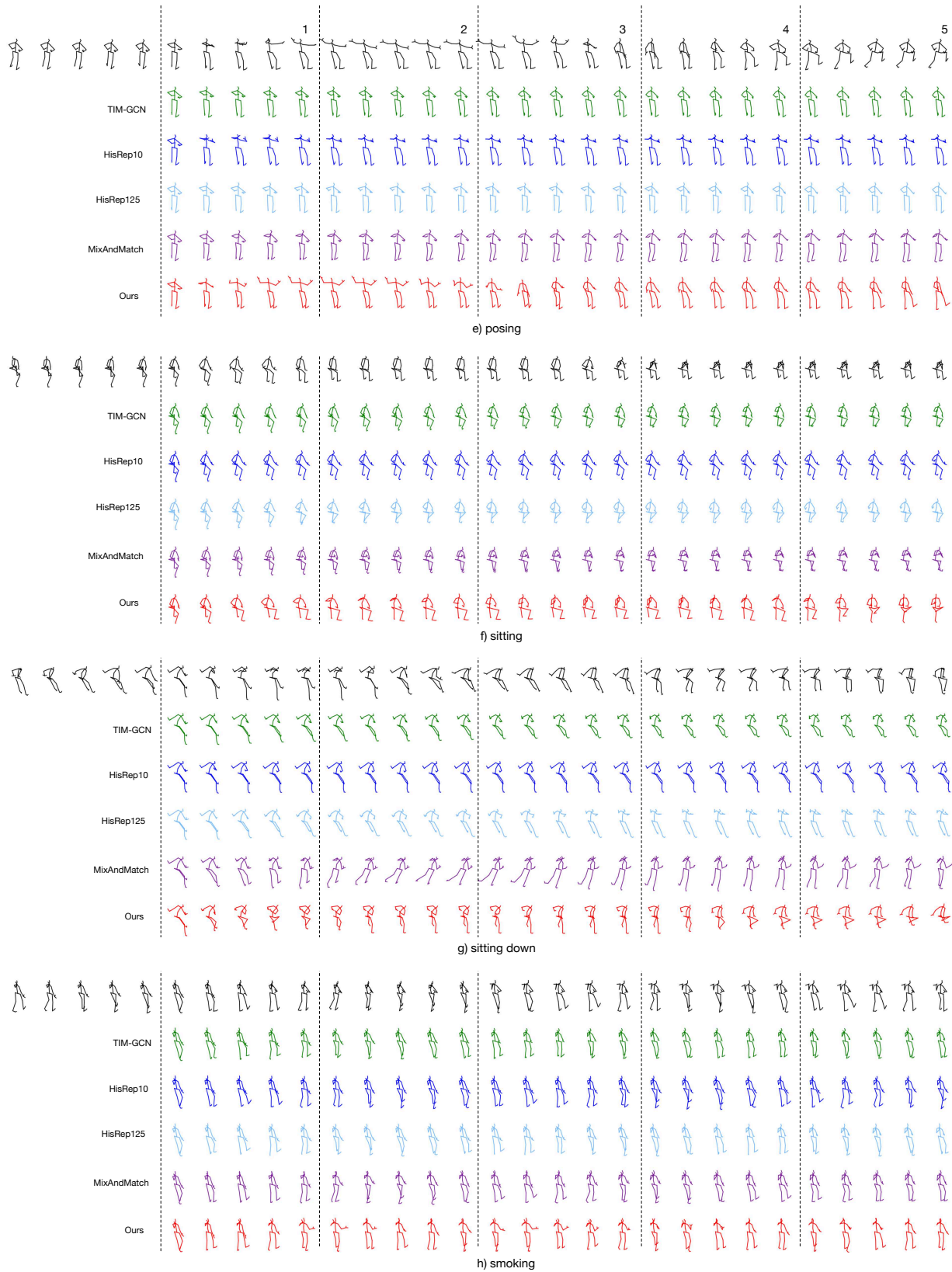


Figure 9. Qualitative results on Human3.6M of actions "posing", "sitting", "sitting down", "smoking".

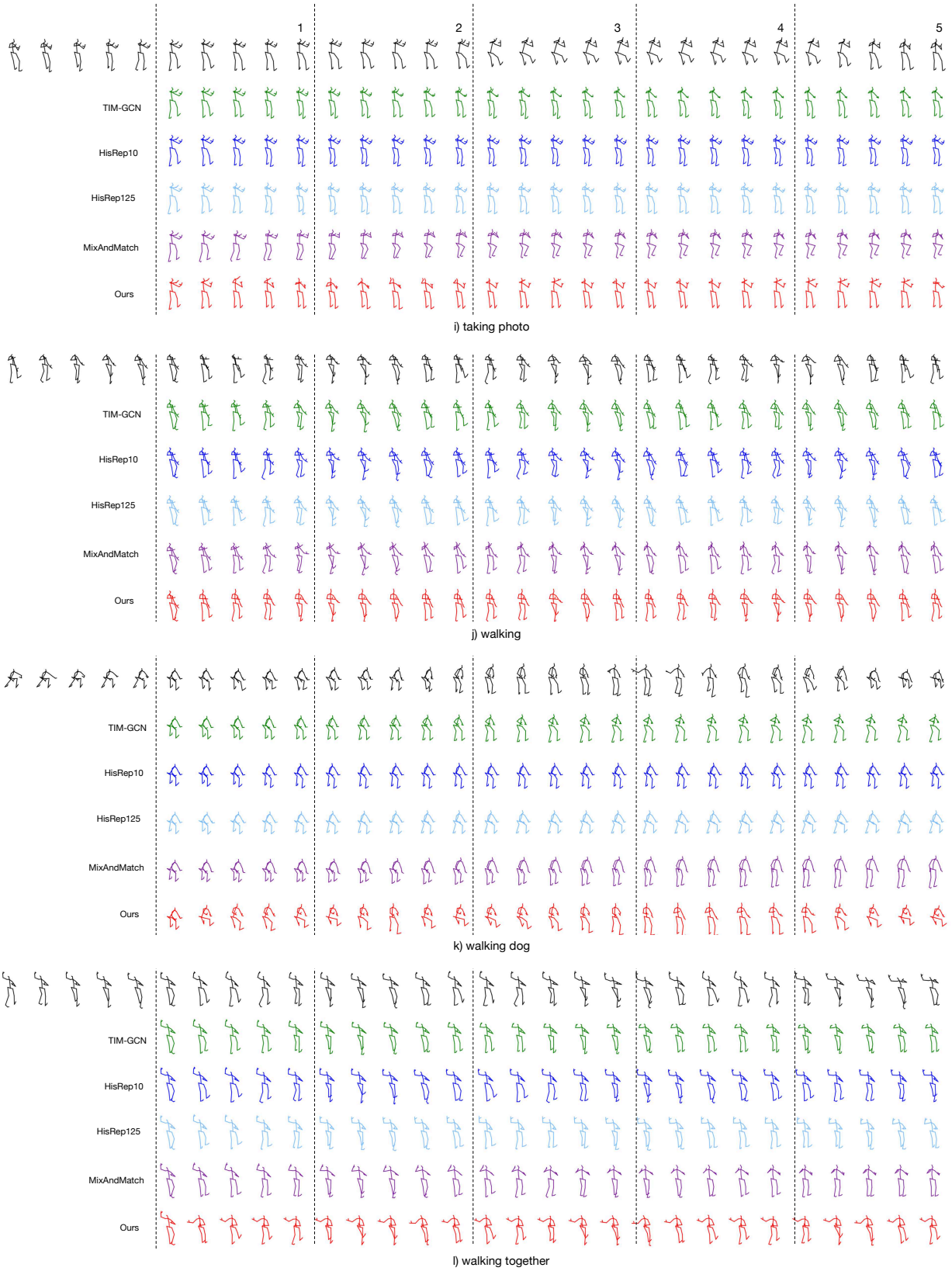


Figure 10. **Qualitative results on Human3.6M** of actions "taking photo", "walking", "walking dog", "walking together".

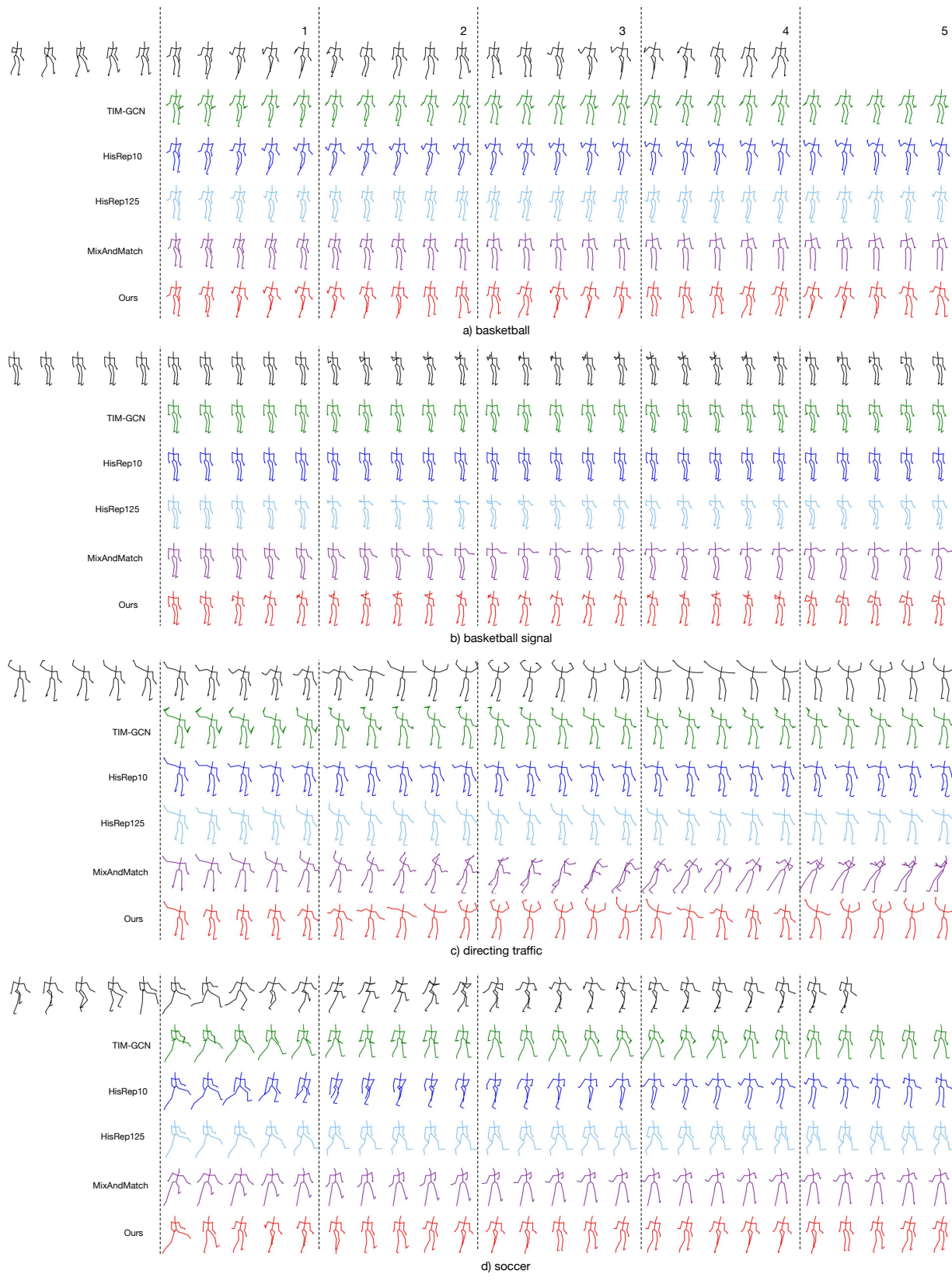


Figure 11. **Qualitative results on CMU Mocap** of actions "basketball", "basketball signal", "directing traffic", "soccer". We draw attention to the legs in basketball, the hands in basketball signal, the wide arm gestures in directing traffic and the legs in soccer.

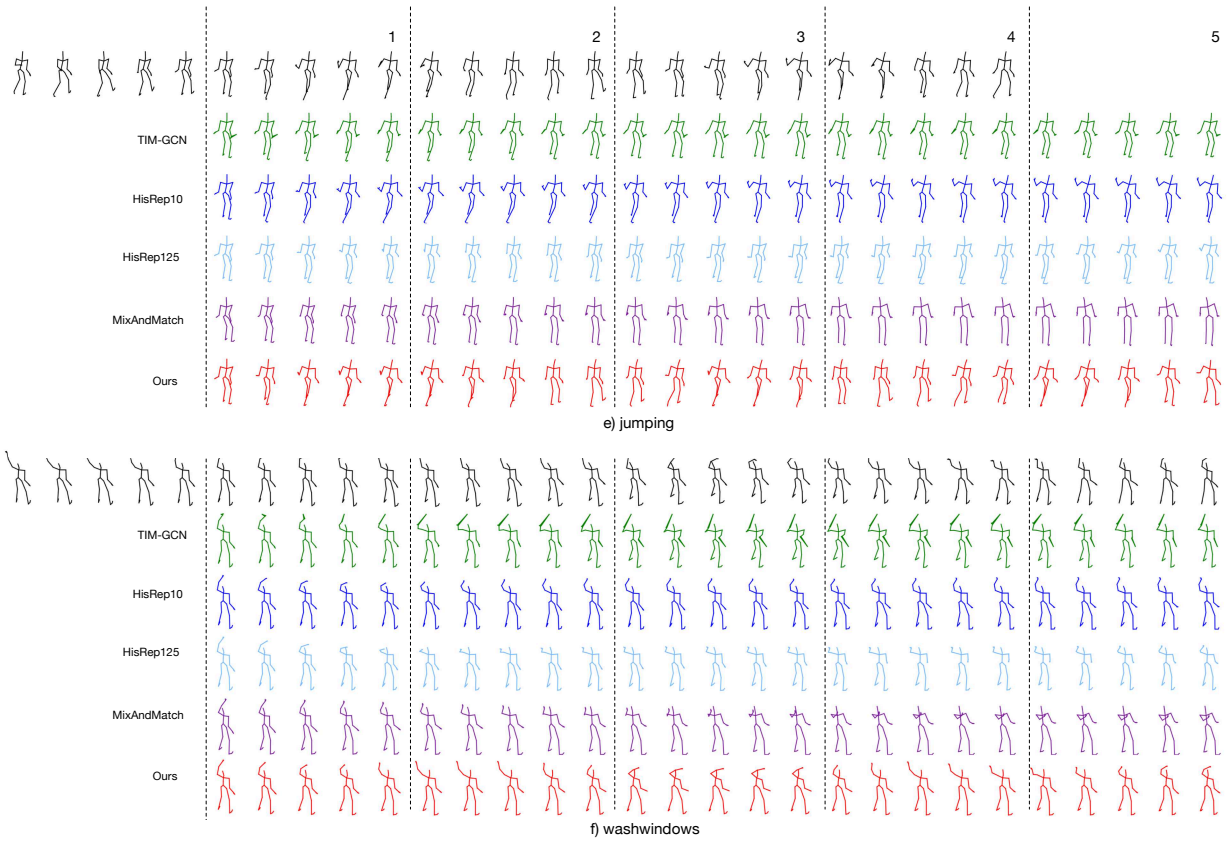


Figure 12. **Qualitative results on CMU Mocap** of actions "jumping","washwindows". We draw attention to the legs in jumping and the arms in washwindows.